Optics Communications 285 (2012) 1269–1274

Contents lists available at SciVerse ScienceDirect

Optics Communications

journal homepage: www.elsevier.com/locate/optcom

Study of the effect of pump focusing on the performance of ghost imaging and ghost diffraction, based on spontaneous parametric downconversion

Daniel R. Guido [b], Alfred B. U'Ren [a,b,*]

[a] Instituto de Ciencias Nucleares, Universidad Nacional Autonoma de Mexico, apdo. postal 70–543, Mexico 04510 DF, Mexico
[b] Departamento de Optica, Centro de Investigación Científica y de Educación Superior de Ensenada, Apartado Postal 2732, Ensenada, BC 22860, Mexico

ARTICLE INFO

Article history:
Received 13 June 2011
Received in revised form 15 September 2011
Accepted 28 September 2011
Available online 11 October 2011

ABSTRACT

We study the effects of ghost imaging (GI) and ghost diffraction (GD), based on spontaneous parametric downconversion (SPDC) photon-pair sources. In particular, we focus on the effect of pump focusing in the SPDC process, on GI and GD. Our theory presented in this paper includes the cases of frequency-degenerate and frequency non-degenerate SPDC. We show analytically, and confirm through numerical simulations, that pump focusing degrades the performance of GI and GD, and for a sufficient focusing strength can altogether suppress these effects.

1. Introduction

Ghost imaging (GI) and ghost diffraction (GD) have inspired much research since their first experimental demonstrations in the mid 1990's [1,2]. These phenomena rely on the spatial correlations present in signal and idler photon-pairs produced by spontaneous parametric downconversion (SPDC) in a nonlinear crystal. In typical GI and GD experiments, while the signal photon traverses a simple optical setup without spatial resolution, the idler photon is spatially resolved upon detection. Spatial correlations between the signal and idler modes, which can become one-to-one under idealized phase-matching conditions, imply that the rate of coincident detection, as a function of the position of the idler detector, can form an image (in the case of GI) or a diffraction pattern (in the case of GD) of an aperture mask placed in the path of the signal photon.

The experimental and theoretical study of GI and GD has stimulated important discussions about the boundary between quantum and classical effects [3–12]. More recently, GI has been studied in the context of thermal illumination rather than SPDC photon-pair illumination [13–16]. With a large number of works from several groups, this area of research has reached a certain level of maturity. As experimental implementations increasingly focus on optimization, and as attention shifts towards applications of these phenomena, future works will benefit from a quantitative understanding of how experimental imperfections may affect the imaging/diffraction performance.

An important aspect in the performance of SPDC sources is the effect of finite transverse dimensions and/or wavefront curvature of the pump beam [17–19]; previous works have studied this in the specific context of GI and GD. Thus, in Ref. [2], the authors found that the inclusion of a transverse pump momentum distribution in their modeling of a GD experiment was necessary in order to obtain good agreement with their experimental measurements. In the case of GI, while setups often involve the use of an imaging lens, interestingly, it has been found in Ref. [20] that the presence of pump focusing can lead to imaging involving specific signal and idler detection planes without the need for an imaging lens. The authors have shown that this GI effect can be observed if an imaging condition, associated with a fictitious spherical mirror with a radius of curvature defined by the pump focusing strength, is satisfied. Also, in a study of the role of entanglement in GI [3], the effect of an arbitrary transverse momentum pump distribution on the resulting type of spatial entanglement has been analyzed.

In the process of SPDC, the annihilation of a single photon from the pump mode, and the resulting generation of a photon pair in the signal and idler modes is subject to energy and momentum conservation. However, it is well known that momentum conservation for SPDC is not exact. Rather, the allowed deviation from perfect longitudinal momentum conservation is governed by the crystal thickness, where an infinitely long crystal would lead to perfect longitudinal momentum conservation. Likewise, the deviation from perfect transverse momentum conservation is governed by the transverse dimensions of the pump beam, where an idealized plane-wave pump would lead to perfect transverse momentum conservation [21,22].

The phenomena of ghost imaging and ghost diffraction, based on photon pairs produced by SPDC, are made possible by near perfect transverse momentum conservation, so that the transverse momenta for the signal and idler photons $\boldsymbol{q}_s$ and $\boldsymbol{q}_i$ fulfil the relation $\boldsymbol{q}_s = -\boldsymbol{q}_i$. Note that the signal and idler modes may be characterized by a spread of allowed transverse momentum values, resulting from the phase-matching characteristics. Perfect transverse momentum conservation

* Corresponding author at: Instituto de Ciencias Nucleares, Universidad Nacional Autonoma de Mexico, apdo. postal 70–543, Mexico 04510 DF, Mexico. Tel.: +52 55 56224739.
E-mail address: alfred.uren@nucleares.unam.mx (A.B. U'Ren).

0030-4018/$ – see front matter © 2011 Elsevier B.V. All rights reserved.
doi:10.1016/j.optcom.2011.09.059

then implies a one-to-one correspondence between each $\boldsymbol{q}_s$ value within the allowed spread of values and each $\boldsymbol{q}_i$ value within the respective allowed spread of values. This leads to the following ray-based interpretation to the photon-pair generation process: reversing the direction of propagation of, say, the signal mode so that light propagates from the detector towards the crystal, perfect transverse momentum conservation implies that each backwards-propagating signal k-vector is "converted" to a corresponding well-defined forward-propagating idler k-vector. This forms the basis for the interpretation of GI and GD experiments in terms of an equivalent geometrical optics construct [23,24].

It is of interest to study how a controlled deviation from perfect transverse momentum conservation affects the performance of ghost imaging and ghost diffraction experiments. In a realistic situation, returning to the above ray-based picture, a single backwards-propagating signal mode is correlated to a *spread* of forward-propagating idler k-vectors, rather than to a *single* idler k-vector. In this paper we analyze experimental situations, closely based on the original implementations of GI and GD from Refs. [1,2], in the presence of pump focusing. We present theoretical results which show how the deviation from perfect transverse momentum conservation which can be controlled by the pump beam width, modeled here as a Gaussian beam, degrades or even suppresses the observation of GI and GD. We arrive at a condition $D=0$ for GI to be observed, with complex D, where $Re(D)=0$ corresponds to the usual thin-lens imaging condition and where $Im(D)=0$ can only be attained in the plane-wave pump limit. We arrive at specific formulae which clarify how a non-zero $Im(D)$ leads to a loss of resolution together with a reduction of the maximum transverse extent of the ghost image. We find that pump focusing leads to similar effects for the case of GD.

In this paper, we concentrate on photon-pair sources based on type-I, non-collinear phasematching and involving a monochromatic pump. While we focus on the case of a Gaussian-beam pump, we also indicate how the calculation would proceed for a more general class of pump beams, including those that have a Gaussian transverse momentum distribution, modulated by an arbitrary function. The results obtained here would be similar for other types of source, including those based on collinear type-II phasematching which was the configuration used for the first experimental demonstration of GI by Pittman et al. [1]. Likewise, in this paper we work within the thin-crystal approximation, for which the spatial dependence of the biphoton wavefunction is considerably simplified. Also, in order to suppress the spectral degree of freedom, and concentrate on spatial variables, we assume that each of the signal and idler modes propagates through narrowband spectral filters.

2. Theory of ghost imaging and ghost diffraction

The quantum state which describes photon pairs produced by spontaneous parametric downconversion may be written as $|\Psi\rangle = |0\rangle + \kappa|\Psi_2\rangle$, in terms of a coefficient related to the conversion efficiency κ and the two-photon component of the state $|\Psi_2\rangle$, given by

$$\left|\Psi_2\right\rangle = \int d\mathbf{q}_s \int d\mathbf{q}_i F(\mathbf{q}_s,\mathbf{q}_i)\left|\mathbf{q}_s\right\rangle\left|\mathbf{q}_i\right\rangle \tag{1}$$

where $|\mathbf{q}_\mu\rangle \equiv a_\mu^\dagger(\mathbf{q}_\mu)|0\rangle$ (with $\mu = s,i$), written in terms of creation operators $a_\mu^\dagger(\mathbf{q}_\mu)$ which are labeled by the transverse momentum $\mathbf{q}_\mu$ for each of the two modes. Note that these transverse momentum variables are defined, for each of the two photons, with respect to a coordinate system for which the z axis is parallel to the direction of propagation characterized by perfect phasematching; our analysis to be presented here is then in terms of the ρ_x and ρ_y transverse coordinates (or q_x and q_y transverse momentum components) for each of the two SPDC modes. Note also that in this description we ignore the spectral degree of freedom; we assume that the signal and idler photons propagate through idealized narrow-band spectral filters, so that a single frequency for each of the two modes (ω_s and ω_i) reaches the detectors.

In Eq. (1), the two-photon component of the state is determined by the biphoton joint amplitude $F(\mathbf{q}_s,\mathbf{q}_i)$. For the specific case of a transverse pump momentum $\mathbf{q}_p$ distribution corresponding to a Gaussian-beam pump of radius w_0, and modulated by a function $\Xi(\mathbf{q}_p)$, $F(\mathbf{q}_s,\mathbf{q}_i)$ can be shown to be given by

$$F(\mathbf{q}_s,\mathbf{q}_i) = \Xi(\mathbf{q}_s+\mathbf{q}_i)\mathrm{sinc}\left(\frac{L}{2}\Delta k(\mathbf{q}_s,\mathbf{q}_i)\right) \times exp\left(-w_0^2\left|\boldsymbol{q}_s+\boldsymbol{q}_i\right|^2_4\right) \tag{2}$$

where L is the crystal length and $\Delta k(\mathbf{q}_s,\mathbf{q}_i)$ is the phase mismatch between the three interacting waves, expressed as

$$\Delta k(\mathbf{q}_s,\mathbf{q}_i) = k_{pz} - k_{sz} - k_{iz} - \left|\mathbf{q}_s+\mathbf{q}_i\right|^2_{2k_p} \tag{3}$$

in terms of the z components of the k-vectors for each of the interacting waves $k_{\mu z}$ (with $\mu = p,s,i$), and the magnitude of the pump k-vector k_p. Note that for an (unmodulated) Gaussian pump beam, $\Xi(\boldsymbol{q}_s+\boldsymbol{q}_i)=1$ and Eq. (2) reduces to the result obtained in Ref. [22]. Through the function $\Xi(\mathbf{q}_p)$ we may include in our analysis, for example, the cases of Hermite–Gauss and Laguerre Gauss pump beams (which represent particular cases of the more general family of Ince–Gauss beams [25]), as well as the cases of Bessel–Gauss and Matthieu–Gauss pump beams [26]. In this paper we work in the thin-crystal limit, for which the sinc function which appears in Eq. (2) can be substituted by unity. Note that the effect of Poynting vector walk off has been neglected in Eq. (2), an approximation which is warranted in the thin-crystal limit.

In order to obtain a theoretical description of ghost imaging and ghost diffraction, our first task is to propagate the biphoton joint amplitude function $F(\mathbf{q}_s,\mathbf{q}_i)$ from the nonlinear crystal through the respective optical elements along the paths of the signal and idler modes in order to reach the detection planes. Thus, in order to proceed with our analysis, we first describe the properties of the photon pairs upon propagation of each of the two photons through an arbitrary optical system. We characterize the optical system through which the signal [idler] photon propagates through the corresponding optical transfer function (OTF) $H_s(\boldsymbol{\rho}_1;\mathbf{q}_s)$ [$H_i(\boldsymbol{\rho}_2;\mathbf{q}_i)$]. Note that while we use subscripts s and i to denote the initial planes (at the output of the crystal), we use subscripts 1 and 2 to denote the final planes, after propagation. In terms of these OTF's, we can write the propagated biphoton joint amplitude $\tilde{F}'(\boldsymbol{\rho}_1,\boldsymbol{\rho}_2)$, in the position (rather than transverse momentum) representation, as [27].

$$\tilde{F}'(\boldsymbol{\rho}_1,\boldsymbol{\rho}_2) \propto \int d\boldsymbol{q}_s \int d\boldsymbol{q}_i H_s(\boldsymbol{\rho}_1;\boldsymbol{q}_s) H_i(\boldsymbol{\rho}_2;\boldsymbol{q}_i) F(\mathbf{q}_s,\mathbf{q}_i) \tag{4}$$

in terms of the biphoton state in the transverse-momentum representation at the output face of the crystal $F(\mathbf{q}_s,\mathbf{q}_i)$. This is illustrated in Fig. 1, where we show the SPDC source, together with the optical systems through which each of the photons propagate, and the detection planes. In the calculations related to ghost imaging and ghost diffraction, to be presented below, we will be particularly interested in the rate of coincidences $R(\boldsymbol{\rho}_1,\boldsymbol{\rho}_2)$, expressed as:

$$R(\boldsymbol{\rho}_1,\boldsymbol{\rho}_2) \equiv \langle\Psi|a(\boldsymbol{\rho}_2)^\dagger a(\boldsymbol{\rho}_1)^\dagger a(\boldsymbol{\rho}_1) a(\boldsymbol{\rho}_2)|\Psi\rangle = \left|\tilde{F}'(\boldsymbol{\rho}_1,\boldsymbol{\rho}_2)\right|^2. \tag{5}$$

Note that the function $R(\boldsymbol{\rho}_1,\boldsymbol{\rho}_2)$ yields the expected rate of coincidences registered by idealized point-like detectors placed at positions $\boldsymbol{\rho}_1$ and $\boldsymbol{\rho}_2$, on detection planes D1 and D2, respectively.

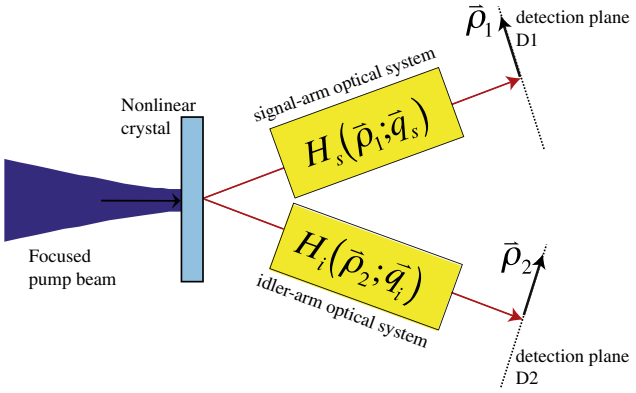

Fig. 1. Schematic showing SPDC photon-pair source, and propagation of the signal and idler modes through arbitrary optical systems.

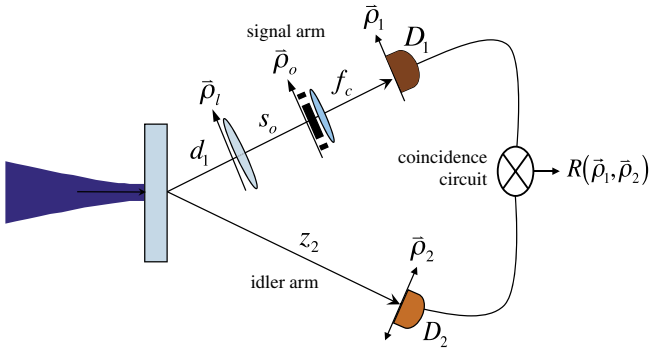

Fig. 2. Ghost imaging setup.

The OTF corresponding to mode μ (with $\mu=s$ for the signal photon and $\mu=i$ for the idler photon) for free-space propagation over distance ℓ, from a plane with transverse coordinates $\boldsymbol{\rho}_0$, to a plane with transverse coordinates ρ in the Fresnel approximation is given by [28,29]

$$H_\mu(\boldsymbol{\rho};\boldsymbol{q}_0)=\frac{e^{ik_\mu\ell}}{\ell}\int d\boldsymbol{\rho}_0 A(\boldsymbol{\rho}_0)h\left(|\boldsymbol{\rho}-\boldsymbol{\rho}_0|,\frac{k_\mu}{\ell}\right)\times e^{i\boldsymbol{\rho}_0\cdot\boldsymbol{q}_0}, \tag{6}$$

written in terms of the k-number k_μ, a possible aperture placed on the plane with coordinate $\boldsymbol{\rho}_0$, $A(\boldsymbol{\rho}_0)$, and of the Fresnel phase factor h ($|\boldsymbol{\alpha}|,\beta$), given by

$$h(|\boldsymbol{\alpha}|,\beta)=exp\left(i\frac{\beta}{2}\left|\boldsymbol{\alpha}\right|^2\right). \tag{7}$$

If propagation involves n stages, with an aperture function $A_i(\rho_i)$ at the initial plane of propagation for each stage, described by coordinate $\boldsymbol{\rho}_i$ (with $i=0,1,2\ldots n-1$) and separated from the subsequent plane by distance ℓ_i, the OTF becomes

$$\begin{aligned}H_\mu\left(\boldsymbol{\rho}_n;\boldsymbol{q}_\mu\right)&=\int d\boldsymbol{\rho}_{n-1}\ldots\int d\boldsymbol{\rho}_0\\&\times A_{n-1}(\boldsymbol{\rho}_{n-1})h(|\boldsymbol{\rho}_n-\boldsymbol{\rho}_{n-1}|,\frac{k_\mu}{\ell_{n-1}})\\&\ldots\times A_0(\boldsymbol{\rho}_0)h(|\boldsymbol{\rho}_1-\boldsymbol{\rho}_0|,\frac{k_\mu}{\ell_0})e^{i\boldsymbol{\rho}_0\cdot\boldsymbol{q}_\mu},\end{aligned} \tag{8}$$

where $\ell_T=\ell_0+\ell_1+\ldots\ell_{n-1}$.

Within this framework, we can now proceed in the next two subsections to study the effects of ghost imaging and ghost diffraction. To this end, we will calculate the specific OTF functions for the signal and idler modes, which describe these specific experimental situations. This will form the basis for our study of the performance of ghost imaging and ghost diffraction as a function of the degree of pump focusing.

2.1. Ghost imaging

A schematic for the ghost imaging setup which we have assumed for our calculations is shown in Fig. 2. This setup is similar to the setup used in the first experimental demonstration by Pittman et al. [1]. A Gaussian beam with waist w_0 is used to pump a nonlinear crystal, which we assume is cut for type I, non-collinear phasematching; we allow the signal and idler photons to be frequency non-degenerate, with frequencies ω_s and ω_i. The signal photon propagates over distance d_1 in order to reach a converging lens at a plane with transverse coordinates $\boldsymbol{\rho}_l$, beyond which it propagates over a further distance s_0 in order to reach a plane containing an aperture mask with transverse coordinates $\boldsymbol{\rho}_0$; the mask is described by function $A(\boldsymbol{\rho}_0)$. Directly behind the mask is a collecting lens of focal length f_c with a detector D_1 placed at distance f_c from the lens; the detector plane is described by coordinate $\boldsymbol{\rho}_1$. Note that this arrangement constitutes a "bucket" detector, since ideally (for a vanishing focusing spot size), all light in the signal arm of the apparatus can be collected by an idealized point-like detector at $\boldsymbol{\rho}_1=0$.

In contrast, the idler photon propagates freely and reaches the detector plane, described by coordinate $\boldsymbol{\rho}_2$. An idealized point-like detector D_2, which in practice can be approximated by a displaceable fiber tip leading to a single-photon detector, then scans the detection plane. The resulting rate of coincidences $R(0,\boldsymbol{\rho}_2)$ between a fixed point-like detector D_1 at $\boldsymbol{\rho}_1=0$ and a displaceable point-like detector D_2 placed at $\boldsymbol{\rho}_2$ is then the physical quantity of interest. The phenomenon of ghost imaging manifests itself when this rate of coincidences, as a function of $\boldsymbol{\rho}_2$, reveals a spatial structure which mimics the mask function $A(\boldsymbol{\rho}_0)$.

In the specific case of the ghost imaging setup of Fig. 2, the optical transfer function of the signal-mode optical system is as follows

$$\begin{aligned}H_s(\boldsymbol{\rho}_1;\boldsymbol{q}_s)\propto&\int d\boldsymbol{\rho}_0\int d\boldsymbol{\rho}_l\int d\boldsymbol{\rho}_s e^{i\boldsymbol{q}_s\cdot\boldsymbol{\rho}_s}h\left(|\boldsymbol{\rho}_l-\boldsymbol{\rho}_s|,\frac{k_s}{d_1}\right)\\&\times h\left(|\boldsymbol{\rho}_l|,\frac{-k_s}{f}\right)h\left(|\boldsymbol{\rho}_0-\boldsymbol{\rho}_l|,\frac{k_s}{s_0}\right)\\&\times A(\boldsymbol{\rho}_0)h\left(|\boldsymbol{\rho}_0|,-\frac{k_s}{f_c}\right)h\left(|\boldsymbol{\rho}_1-\boldsymbol{\rho}_0|,\frac{k_s}{f_c}\right),\end{aligned} \tag{9}$$

where we have disregarded constant phase factors, $\boldsymbol{\rho}_s$ is the transverse coordinate at the source, $\boldsymbol{\rho}_l$ and $\boldsymbol{\rho}_0$ are the coordinates on the planes of the imaging lens and aperture mask respectively, $h\left(|\boldsymbol{\rho}_l|,\frac{-k_s}{f}\right)$ is the quadratic phase factor associated with the imaging lens with focal length f, $A(\rho_0)$ represents the aperture mask, and $h\left(|\boldsymbol{\rho}_0|,\frac{-k_s}{f_c}\right)$ is the quadratic phase factor associated with the collection lens. In contrast to the signal mode, the idler mode only experiences free-space propagation from the non-linear crystal to the detection plane. The corresponding OTF can be written as

$$H_i(\boldsymbol{\rho}_2;\boldsymbol{q}_i)\propto\int d\boldsymbol{\rho}_i h\left(|\boldsymbol{\rho}_2-\boldsymbol{\rho}_i|,\frac{k_i}{z_2}\right)e^{i\boldsymbol{q}_i\cdot\boldsymbol{\rho}_i}, \tag{10}$$

where $\boldsymbol{\rho}_i$ is the transverse coordinate at the source. Substituting the OTF's, i.e. Eqs. (9) and (10), into Eq. (5), and after some algebra we can write the resulting coincidence rate at the two detection planes as

$$\begin{aligned}R(\boldsymbol{\rho}_1,\boldsymbol{\rho}_2)\propto&\left|h\left(|\boldsymbol{\rho}_2|,\frac{k_s}{Ms_o}+i\frac{2k_i}{z_2w_0^2\alpha}\right)h\left(|\boldsymbol{\rho}_1|,\frac{k_s}{f_c}\right)\right.\\&\times\int d\boldsymbol{\rho}_0 A(\boldsymbol{\rho}_0)h\left(|\boldsymbol{\rho}_0|,\frac{k_s}{s_0}\right)e^{-i\frac{k_s}{f_c}\boldsymbol{\rho}_1\cdot\boldsymbol{\rho}_0}\\&\left.\times\int d\boldsymbol{\rho}_l h(|\boldsymbol{\rho}_l|,D)e^{-i\left(\frac{k_s}{Ms_o}\boldsymbol{\rho}_2+\frac{k_s}{s_o}\boldsymbol{\rho}_0\right)\cdot\boldsymbol{\rho}_l}\right|^2,\end{aligned} \tag{11}$$

where $\alpha=k_s/d_1+k_i/z_2$, and where M represents the magnification

factor given by

$$M = \frac{\frac{\omega_s}{\omega_i} z_2 + d_1}{s_o}. \tag{12}$$

In Eq. (11), parameter D is given by

$$D = k_s \left(\frac{1}{\frac{\omega_s}{\omega_i} z_2 + d_1} + \frac{1}{s_0} - \frac{1}{f} + i \frac{2}{d_1 w_0^2 \alpha} \right), \tag{13}$$

and is related to the imaging condition (for the lens with focal length f) and to the effect of a finite beam waist w_0. Note that D is a complex quantity and that its imaginary part vanishes in the limit where the pump is a plane wave, i.e. $w_0 \to \infty$. It is convenient to define an imaging distance s_i as follows

$$s_i = \frac{\omega_s}{\omega_i} z_2 + d_1, \tag{14}$$

which clearly reduces to $s_i = z_2 + d_1$ in the frequency-degenerate case. In terms of s_i, the magnification factor becomes $M = s_i/s_o$. Also, in terms of this imaging distance, we can write parameter α as $\alpha = k_s s_i/(d_1 z_2)$, and parameter D (see Eq. (13)) becomes

$$D = k_s \left(\frac{1}{s_i} + \frac{1}{s_o} - \frac{1}{f} \right) + i \frac{2(s_i - d_1)}{w_0^2 s_i}. \tag{15}$$

Thus, the condition resulting from making the real part of parameter D in Eq. (15) vanish has the form of a thin-lens imaging condition for the lens with focal length f. This condition can be used for defining the position of the appropriate detection plane where imaging occurs, specifically by solving the equation $\mathrm{Re}(D) = 0$, for z_2 (for given values of d_1, s_0 and f). In the degenerate case, this imaging condition is equivalent to an "unfolded" version of the setup where the aperture mask plane, placed at a distance s_0 behind the imaging lens, is imaged to the D2 detector plane, a distance $s_i = d_1 + z_2$ in front of the imaging lens. In the non-degenerate case, this interpretation holds, except that the effective imaging distance is appropriately modified through factor ω_s/ω_i in Eq. (14). Note that recent work has analyzed the question of the attainable resolution in ghost-imaging based on frequency non-degenerate SPDC [30–32]. Our analysis in this paper includes frequency non-degeneracy as well as the effect of pump focusing.

We are particularly interested in the coincidence rate evaluated at $\boldsymbol{\rho}_1 = 0$, i.e. in the function $R(0, \boldsymbol{\rho}_2)$, given by

$$R(0, \boldsymbol{\rho}_2) \propto e^{-\frac{2 d_1 |\boldsymbol{\rho}_2|^2}{w_0^2 s_i}} \left| \int d\boldsymbol{\rho}_0 A(\boldsymbol{\rho}_0) G(\boldsymbol{\rho}_2, \boldsymbol{\rho}_0) \right|^2, \tag{16}$$

in terms of the following definition

$$G(\boldsymbol{\rho}_2, \boldsymbol{\rho}_0) = e^{i \frac{k_s |\boldsymbol{\rho}_0|^2}{2 s_o}} \int d\boldsymbol{\rho}_l e^{i \frac{D}{2} |\boldsymbol{\rho}_l|^2} e^{-i \frac{k_s}{s_o} \left(\frac{1}{M} \boldsymbol{\rho}_2 + \boldsymbol{\rho}_0 \right) \cdot \boldsymbol{\rho}_l}, \tag{17}$$

If we concentrate our discussion on the case for which the imaging condition $\mathrm{Re}(D) = 0$ is fulfilled, the function $G(\rho_2, \rho_0)$ becomes

$$G(\boldsymbol{\rho}_2, \boldsymbol{\rho}_0) = e^{i \frac{k_s |\boldsymbol{\rho}_0|^2}{2 s_o}} \int d\boldsymbol{\rho}_l e^{-\frac{\omega_s}{\omega_i} \frac{z_2}{w_0^2 s_i} |\boldsymbol{\rho}_l|^2} e^{-i \frac{k_s}{s_o} \left(\frac{1}{M} \boldsymbol{\rho}_2 + \boldsymbol{\rho}_0 \right) \cdot \boldsymbol{\rho}_l}. \tag{18}$$

Note that the function $G(\boldsymbol{\rho}_2, \boldsymbol{\rho}_0)$ can be interpreted as a point-spread-function: it represents the response, on the image plane, of the imaging system to a point source, on the plane of the aperture mask. This function has a width which vanishes in the plane-wave limit ($w_0 \to \infty$) and becomes progressively larger as the SPDC pump is focused to a greater degree. Indeed, in the plane wave limit, this function reduces to

$$G(\boldsymbol{\rho}_2, \boldsymbol{\rho}_0) \propto e^{i \frac{k_s |\boldsymbol{\rho}_0|^2}{2 s_o}} \delta \left(\boldsymbol{\rho}_0 + \frac{1}{M} \boldsymbol{\rho}_2 \right), \tag{19}$$

for which imaging occurs in principle ideally with a one-to-one correspondence between the object and image planes.

The multiplicative Gaussian function which appears in Eq. (16) can be interpreted as a resulting aperture function on the image plane; as the SPDC pump is focused to a progressively greater degree, this function further limits the extent of the image. Thus, the effect of a focused pump is two-fold: i) it broadens the point-spread-function $G(\boldsymbol{\rho}_2, \boldsymbol{\rho}_0)$, thus reducing the attainable resolution, and ii) it limits the extent of the reduced-resolution image which can be recovered by displacing a point-like detector D2 and monitoring the rate of coincidences.

Note that modifying the setup from one based on degenerate SPDC to one based on non-degenerate SPDC, while maintaining the values of d_1, s_0, and f and adjusting the distance z_2 so that the condition $\mathrm{Re}(D) = 0$ is still fulfilled, yields an identical magnification factor M, determined by f and s_0 as $M = f/(s_0 - f)$.

2.2. Ghost diffraction

Let us now turn our attention to ghost diffraction. A schematic for the ghost diffraction setup which we have assumed for our calculations is shown in Fig. 3. This setup is similar to the one used in the first experimental demonstration by Strekalov et al. [2]. A Gaussian beam with waist w_0 is used to pump a nonlinear crystal, which we assume is cut for type I, non-collinear phasematching; we allow the signal and idler photons to be frequency non-degenerate, with frequencies ω_s and ω_i. The signal photon propagates through distance d_1 in order to reach a diffracting aperture, characterized by function $A(\boldsymbol{\rho}_0)$, beyond which it propagates through an additional distance d_2 in order to reach a detection plane. While the plane of the mask is described in terms of coordinate $\boldsymbol{\rho}_0$, the final detection plane is described in terms of coordinate $\boldsymbol{\rho}_1$. For the ghost diffraction effect, we will consider a point-like detector on this detection plane, characterized by $\boldsymbol{\rho}_1 = 0$. Note that this is different to the ghost imaging setup, where a collection lens before detector D1 turns this detector into a "bucket detector".

In contrast, the idler photon propagates freely and reaches the detector plane, described by coordinate $\boldsymbol{\rho}_2$. An idealized point-like detector D_2, which can in practice be approximated by a displaceable fiber tip leading to a single-photon detector, then scans the detection plane. The resulting rate of coincidences $R(0, \boldsymbol{\rho}_2)$ between a fixed point-like detector D_1 at $\boldsymbol{\rho}_1 = 0$ and a displaceable point-like detector D_2 placed at $\boldsymbol{\rho}_2$ is then the physical quantity of interest. The phenomenon of ghost diffraction manifests itself when this rate of coincidences, as a function of $\boldsymbol{\rho}_2$, reveals a spatial structure which mimics the Fresnel diffraction pattern obtained over distance $d_1 + z_2$ (as will be discussed below, this diffraction distance is modified in the case of non-degenerate SPDC) of the diffracting aperture $A(\boldsymbol{\rho}_0)$, illuminated by a point light source a distance d_2 from the aperture.

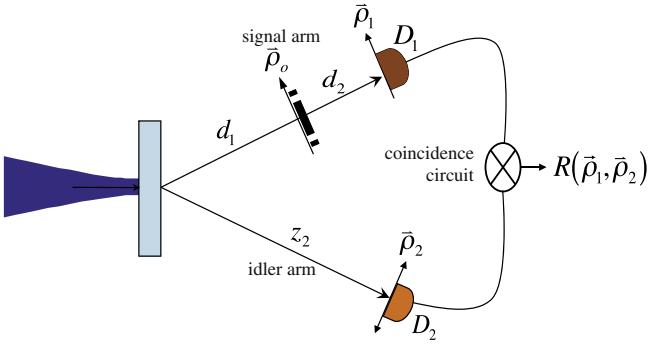

Fig. 3. Ghost diffraction setup.

In order to proceed with our analysis, we write down the OTF for the signal mode

$$H_s(\boldsymbol{\rho}_1;\mathbf{q}_s)\propto\int d\boldsymbol{\rho}_0\int d\boldsymbol{\rho}_s h\left(|\boldsymbol{\rho}_s-\boldsymbol{\rho}_0|,\frac{k_s}{d_1}\right)A(\boldsymbol{\rho}_0)h\left(|\boldsymbol{\rho}_0-\boldsymbol{\rho}_1|,\frac{k_s}{d_2}\right)e^{i\mathbf{q}_s\cdot\boldsymbol{\rho}_s}. \quad (20)$$

Likewise, we write down the OTF for the idler mode

$$H_i(\boldsymbol{\rho}_2;\mathbf{q}_i)\propto\int d\boldsymbol{\rho}_i h\left(|\boldsymbol{\rho}_i-\boldsymbol{\rho}_2|,\frac{k_i}{z_2}\right)e^{i\mathbf{q}_i\cdot\boldsymbol{\rho}_i}. \quad (21)$$

Substituting the OTF's (Eqs. (20) and (21)) into Eq. (5) and after some algebra we can write the resulting coincidence rate at the two detection planes as

$$R(0,\boldsymbol{\rho}_2)\propto e^{-\frac{2d_1}{w_0^2 z_0^2}|\boldsymbol{\rho}_2|^2}\left|\int d\boldsymbol{\rho}_0\left[A(\boldsymbol{\rho}_0)e^{-\frac{(z_0-d_1)}{w_0^2 z_0^2}|\boldsymbol{\rho}_0|^2}e^{i\frac{k_s}{2d_2}|\boldsymbol{\rho}_0|^2}\right]e^{i\frac{k_s}{2z_0}|\boldsymbol{\rho}_0|^2}e^{-i\frac{k_s}{z_0}\boldsymbol{\rho}_0\cdot\boldsymbol{\rho}_2}\right|^2, \quad (22)$$

in terms of the definition

$$z_0=d_1+\frac{\omega_s}{\omega_i}z_2. \quad (23)$$

Note that the expression for the coincidence rate $R(0,\rho_2)$ contains a resulting aperture function defined on the detector plane with coordinate ρ_2, multiplied by the intensity pattern, associated with the Fresnel diffraction of the complex amplitude which appears in square brackets in Eq. (22)[29]. Thus, the system behaves as an equivalent "unfolded system" where the coincidence rate between a fixed point-like detector D1 and a displaceable point-like detector D2, as a function of the position of D2, can represent the Fresnel diffraction pattern of the electric field amplitude on the aperture mask plane, over distance z_0 (see Eq. (23)). Note that the complex amplitude on the aperture mask plane, with coordinate $\boldsymbol{\rho}_0$, also contains an effective aperture function. Both effective aperture functions, on planes with coordinates $\boldsymbol{\rho}_0$ and $\boldsymbol{\rho}_2$, have widths proportional to the pump beam radius w_0. In other words, both of these apertures are suppressed in the plane-wave pump limit ($w_0\to\infty$) and both become more acute for a greater pump focusing strength.

Thus, the effect of pump focusing is two-fold. On the one hand, the resulting aperture function on the aperture mask plane has the effect that for tighter pump focusing, the effective transverse dimensions of the diffracting aperture are reduced, or clipped, when compared to the dimensions of the diffracting mask aperture itself. On the other hand, the resulting intensity distribution on the detection plane D2 is likewise increasingly clipped for greater focusing strengths by the resulting aperture function on this plane. The effect of both apertures is, clearly that strong pump focusing can inhibit the ghost diffraction effect by clipping both the diffracting aperture on the plane of the aperture mask, and the diffraction pattern on the detection plane.

3. Results and discussion

In this section we illustrate our discussion of the previous section with specific examples, directly showing how pump focusing degrades the performance of ghost imaging and ghost diffraction. In particular, we show results obtained by numerical integration of Eq. (16), in the case of ghost imaging, and of Eq. (22) in the case of ghost diffraction.

For these simulations we assume an SPDC photon-pair source based on a beta barium borate (BBO) crystal, with a pump wavelength of 0.35 μm and degenerate-frequency signal and idler modes at $\lambda_s=\lambda_i=0.70$ μm. We assume that the nonlinear crystal is cut for non-collinear phasematching involving signal and idler propagation at angles defined by the resulting phasematching properties. For these illustrations, we have selected an aperture mask in the form of a double slit, both for GI and GD. In particular, the mask which we have assumed is composed of two parallel, rectangular slits of dimensions 0.15×1.1 mm, placed side by side along the long edges of the rectangles, separated from each other, on a center-to-center basis, by 0.47 mm.

Let us first concentrate on the ghost imaging case, relying on frequency-degenerate SPDC. We have selected the following parameters for the signal arm: crystal-imaging lens distance $d_1=600$ mm, imaging-lens focal length $f=400$ mm, imaging lens-aperture mask distance $s_0=600$ mm; note that $R(0,\boldsymbol{\rho}_2)$ is independent of the collection lens focal length f_c. For the idler arm, we have selected the crystal-detection plane D2 distance $z_2=600$ mm. This choice of parameters fulfils the imaging condition $\mathrm{Re}(D)=0$, and results in a magnification parameter (see Eq. (12)) of $M=2$. The resulting expected coincidence rate $R(0,\boldsymbol{\rho}_2)$ is plotted as a function of $\boldsymbol{\rho}_2$ in Fig. 4, where panels (a) through (d) correspond to the following values of w_0: a) $w_0=3$ mm, b) $w_0=1$ mm, c) $w_0=0.5$ mm and d) $w_0=0.3$ mm. These results correspond to the coincidence rate between a fixed, point-like detector D1 (at $\boldsymbol{\rho}_1=0$) and a displaceable point-like detector D2, as a function of the position of D2 $\boldsymbol{\rho}_2$. It is clear from these results that for the largest value of w_0 ($w_0=3$ mm, for which the pump corresponds essentially to a plane wave), function $R(0,\rho_2)$ reveals a spatial structure which closely mimics the aperture mask used, appropriately scaled by the magnification factor ($M=2$ in this case). It is also clear from these results that as the strength of pump focusing is increased (yielding increasingly smaller values of w_0), the ghost imaging effect is degraded. Indeed, for the smallest value of w_0 assumed, the ghost imaging effect is visibly altogether suppressed.

Let us now turn our attention to the ghost diffraction effect, relying on frequency-degenerate SPDC. We have selected the following parameters: crystal-aperture mask distance $d_1=500$ mm, aperture mask-detection plane D1 distance $d_2=500$ mm, and crystal-detection plane D2 distance $z_2=1200$ mm. The resulting expected coincidence rate $R(0,\boldsymbol{\rho}_2)$ is plotted as a function of $\boldsymbol{\rho}_2$ in Fig. 5, where panels (a) through (d) correspond to the following values for w_0: a) $w_0=3$ mm, b) $w_0=2.5$ mm, c) $w_0=1$ mm and d) $w_0=0.5$ mm. These results correspond to the

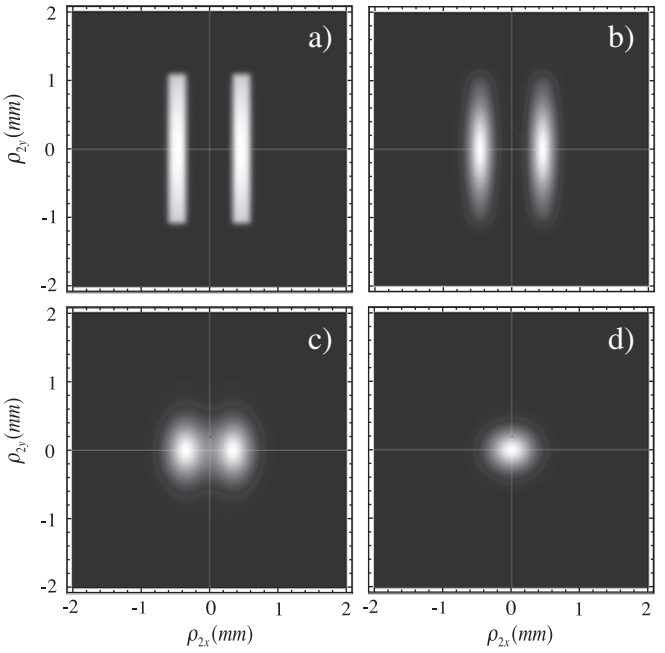

Fig. 4. Plots of the coincidence rate $R(0,\boldsymbol{\rho}_2)$ for the ghost imaging effect, relying on frequency-degenerate SPDC. We have assumed the following values for the pump beam radius: a)$w_0=3$ mm, b)$w_0=1$ mm, c)$w_0=0.5$ mm and d)$w_0=0.3$ mm.

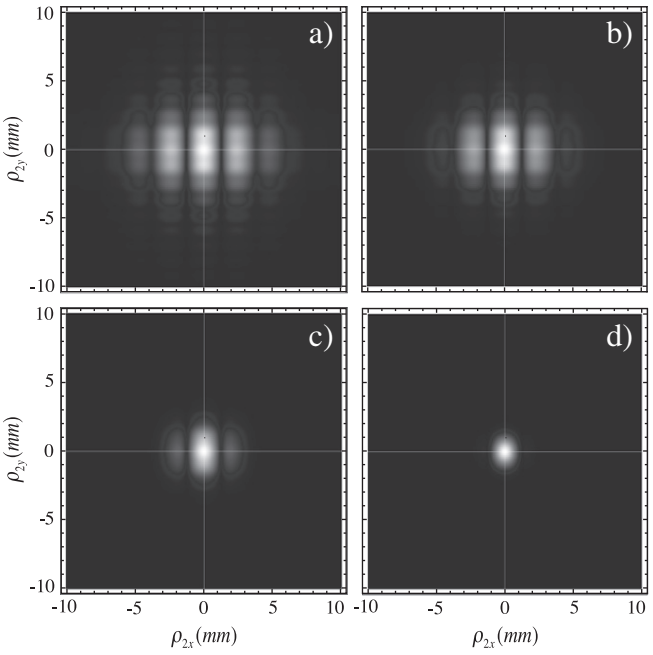

Fig. 5. Plots of the coincidence rate $R(0,\boldsymbol{\rho}_2)$ for the ghost diffraction effect, relying on frequency-degenerate SPDC. We have assumed the following values for the pump beam radius: a)$w_0=3$ mm, b)$w_0=2.5$ mm, c)$w_0=1$ mm and d)$w_0=0.5$ mm.

coincidence rate between a fixed, point-like detector D1 (at $\boldsymbol{\rho}_1=0$) and a displaceable point-like detector D2, as a function of the position of D2 $\boldsymbol{\rho}_2$. For the largest value of w_0 ($w_0=3$ mm, for which the pump corresponds essentially to a plane wave), function $R(0,\boldsymbol{\rho}_2)$ reveals a spatial structure which essentially corresponds to the Fresnel diffraction pattern of the aperture mask used, over distance d_1+z_2. It is clear from the figure that as the strength of pump focusing is increased (yielding increasingly smaller values of w_0), the ghost diffraction effect is degraded. In particular, as w_0 is decreased, diffraction orders are lost, as is clear from panels C and D.

4. Conclusions

We have studied the phenomena of ghost imaging (GI) and ghost diffraction (GD), based on spontaneous parametric downconversion (SPDC) photon-pair sources. In our analysis we have explicitly taken into account the propagation of the SPDC biphotons through the various optical elements involved in these two experiments, in order to reach the two detection planes. Based on this analysis, we have obtained analytic expressions for the rate of coincidences expected between two point-like detectors placed on each of these planes, as a function of the positions of the detectors. These expressions, which are in the form of integrals which can be computed numerically, are general enough to include the case of an arbitrary degree of pump focusing in the SPDC process, where the pump beam is modelled as a Gaussian beam. These expressions are likewise general enough to include the case of arbitrarily frequency non-degenerate signal and idler modes. In addition we have indicated how the calculation would proceed if the pump transverse momentum distribution corresponds to that of a Gaussian beam, modulated by an arbitrary function.

In general, because GI and GD rely on spatial correlations between the signal and idler photons, and because these correlations are weakened as the SPDC-process pump beam is focused, one would expect that pump focusing would tend to inhibit the GI and GD effects. Our analysis (analytic and numerical) explicitly shows how a deviation from the perfect transverse signal-idler correlations, controlled by the degree of pump focusing, indeed degrades the GI and GD effects. The results described in this paper lead to an enhanced understanding of the GI and GD effects under realistic experimental conditions, and may lead to optimized experimental implementations.

Acknowledgements

This work was supported in part by CONACYT, Mexico, by DGAPA, UNAM and by FONCICYT project 94142.

References

[1] T.B. Pittman, Y.H. Shih, D.V. Strekalov, A.V. Sergienko, Physical Review A 52 (1995) R3429.
[2] D.V. Strekalov, A.V. Sergienko, D.N. Klyshko, Y.H. Shih, Physical Review Letters 74 (1995) 3600.
[3] A.F. Abouraddy, B.E.A. Saleh, A.V. Sergienko, M.C. Teich, Physical Review Letters 87 (2001) 123602.
[4] R.S. Bennink, S.J. Bentley, R.W. Boyd, Physical Review Letters 89 (84) (2002) 113601.
[5] R.S. Bennink, S.J. Bentley, R.W. Boyd, J.C. Howell, Physical Review Letters 92 (2004) 033601.
[6] A. Gatti, E. Brambilla, M. Bache, L.A. Lugiato, Physical Review Letters 93 (2004) 093602.
[7] M. D'Angelo, Y.H. Kim, S.P. Kulik, Y.H. Shih, Physical Review Letters 92 (2004) 233601.
[8] M. D'Angelo, A. Valencia, M.H. Rubin, Y. Shih, Physical Review A 72 (2005) 013810.
[9] Y. Cai, S.Y. Zhu, Physical Review E 71 (2005) 056607.
[10] G. Scarcelli, V. Berardi, Y. Shih, Physical Review Letters 96 (2006) 063602.
[11] I.F. Santos, J.G. Aguirre Gomez, S. Padua, Physical Review A 77 (2008) 043832.
[12] B.I. Erkmen, J.H. Shapiro, Physical Review A 77 (2008) 043809.
[13] A. Valencia, G. Scarcelli, M. D'Angelo, Y. Shih, Physical Review Letters 94 (2005) 063601.
[14] F. Ferri, D. Magatti, A. Gatti, M. Bache, E. Brambilla, L.A. Lugiato, Physical Review Letters 94 (2005) 183602.
[15] Y. Bromberg, O. Katz, Y. Silberberg, Physical Review A 79 (2009) 053840.
[16] M. Zhang, Q. Wei, X. Shen, Y. Liu, H. Liu, J. Chen, S. Han, Physical Review A 75 (2007) 021803 (R).
[17] P.S.K. Lee, M.P. van Exter, J.P. Woerdman, Physical Review A 72 (2005) 033803.
[18] G. Molina-Terriza, S. Minardi, Y. Deyanova, C.I. Osorio, M. Hendrych, J.P. Torres, Physical Review A 72 (2005) 065802.
[19] A.V. Burlakov, M.V. Chekhova, D.N. Klyshko, S.P. Kulik, A.N. Penin, Y.H. Shih, D.V. Strekalov, Physical Review A 56 (1997) 3214.
[20] T.B. Pittman, D.V. Strekalov, D.N. Klyshko, M.H. Rubin, A.V. Sergienko, Y.H. Shih, Physical Review A 53 (1996) 2804.
[21] M.H. Rubin, Physical Review A 54 (1996) 5349.
[22] L.E. Vicent, A.B. U'Ren, R. Rangarajan, C.I. Osorio, J.P. Torres, L. Zhang, I.A. Walmsley, New Journal of Physics 12 (2010) 093027.
[23] D.N. Klyshko, Physics Letters A 132 (1998) 299.
[24] O. Steuernagel, H. Rabitz, Optics Communication 154 (1998) 285.
[25] M.A. Bandres, J.C. Gutierrez-Vega, Optics Letters 29 (2004) 144.
[26] J.C. Gutierrez-Vega, M.A. Bandres, Journal of the Optical Society of America. A 22 (2005) 289.
[27] B.E.A. Saleh, A.F. Abouraddy, A.V. Sergienko, M.C. Teich, Physical Review A 62 (2000) 043816.
[28] Y. Shih, arXiv:0706.2097v2[quant-ph], 2007.
[29] J.W. Goodman, Introduction to Fourier Optics, McGraw-Hill Publishing, 1968.
[30] M.H. Rubin, Y. Shih, Physical Review A 78 (2008) 033836.
[31] K.W.C. Chan, M.N. O'Sullivan, R.W. Boyd, Physical Review A 79 (2009) 033808.
[32] S. Karmakar, Y. Shih, Physical Review A 81 (2010) 033845.